OXFORD

Cerebral Cortex, 2022, **32**, 2943–2956
https://doi.org/10.1093/cercor/bhab392
Advance access publication date: 2 November 2021
Original Article

Laterality hotspots in the striatum

Cole Korponay [1,*], Elliot A. Stein[2], Thomas J. Ross[2]

[1]Basic Neuroscience Division, McLean Hospital, Belmont, MA 02478, USA,
[2]Neuroimaging Research Branch, Intramural Research Program, National Institute on Drug Abuse, Baltimore, MD 21224, USA

*Corresponding author: Cole Korponay. Email: ckorponay@mclean.harvard.edu

Striatal loci are connected to both the ipsilateral and contralateral frontal cortex. Normative quantitation of the dissimilarity between striatal loci's hemispheric connection profiles and its spatial variance across the striatum, and assessment of how interindividual differences relate to function, stands to further the understanding of the role of corticostriatal circuits in lateralized functions and the role of abnormal corticostriatal laterality in neurodevelopmental and other neuropsychiatric disorders. A resting-state functional connectivity fingerprinting approach ($n = 261$) identified "laterality hotspots"—loci whose profiles of connectivity with ipsilateral and contralateral frontal cortex were disproportionately dissimilar—in the right rostral ventral putamen, left rostral central caudate, and bilateral caudal ventral caudate. Findings were replicated in an independent sample and were robust to both preprocessing choices and the choice of cortical atlas used for parcellation definitions. Across subjects, greater rightward connectional laterality at the right ventral putamen hotspot and greater leftward connectional laterality at the left rostral caudate hotspot were associated with higher performance on tasks engaging lateralized functions (i.e., response inhibition and language, respectively). In sum, we find robust and reproducible evidence for striatal loci with disproportionately lateralized connectivity profiles where interindividual differences in laterality magnitude are associated with behavioral capacities on lateralized functions.

Key words: connectivity; frontostriatal; inhibition; language; laterality.

Introduction

Asymmetries between the left and right hemispheres of the brain constitute a fundamental feature of neural organization. These asymmetries, which manifest both in gross anatomy and in structural and functional connections, contribute to the neural basis of lateralized brain functions (Corballis 2017), including notably language (Kelly et al. 2010), inhibitory control (Garavan et al. 1999; Aron et al. 2014), and salience detection (Kucyi et al. 2012). An abnormal magnitude of hemispheric asymmetry (i.e., laterality) in neural substrates and functional connectivity (FC) is a shared feature of numerous neurodevelopmental and psychiatric disorders, including autism spectrum disorders (ASDs), attention-deficit/hyperactivity disorder (ADHD), and schizophrenia (Bradshaw and Sheppard 2000; Berretz et al. 2020). Individuals with schizophrenia, for instance, have reduced leftward structural (Sommer et al. 2001; Miyata et al. 2012) and FC (Swanson et al. 2011) asymmetry (i.e., more symmetry) compared with healthy individuals. Common across many of these disorders is atypical asymmetry in frontal corticostriatal circuitry in particular (Bradshaw and Sheppard 2000; Cao et al. 2016; Silk et al. 2016). Individuals with ASDs have reduced leftward asymmetries or reversed asymmetries in frontal cortical language regions, with more atypical asymmetry associated with greater language deficits (Lindell and Hudry 2013). Youths with ADHD have reduced rightward asymmetry in caudate-ventrolateral prefrontal cortex and caudate-dorsolateral prefrontal cortex white matter tract volume compared with controls (Silk et al. 2016). In a recent mega-analysis of 22 structural brain MRI datasets, substance dependence was found to be associated with reduced rightward structural asymmetry of the nucleus accumbens (Cao et al. 2016).

Most prior studies have evaluated laterality by comparing individual pairs of brain regions or connections. However, a dimension of laterality that has been relatively underexplored is that pertaining to FC profiles. A brain area's FC profile, or "fingerprint," is the multivariate set of connection strengths it has with other areas of the brain (Passingham et al. 2002; Mars et al. 2016). The value of examining FC profiles is that, more so than any one particular connection, it is the combinatorial makeup of a brain area's full set of connections that most shapes its activity and function (Passingham et al. 2002). However, there has been little examination of laterality in FC profiles, including whether its magnitude varies spatially within the brain and whether intersubject variation relates to capacities in lateralized cognitive functions like language. Investigating these questions—particularly in corticostriatal circuitry, where atypical laterality is frequently implicated in neuropsychiatric

Received: June 10, 2021. **Revised:** September 30, 2021. **Accepted:** October 1, 2021
Published by Oxford University Press 2021.

disease (Bradshaw and Sheppard 2000; Cao et al. 2016; Silk et al. 2016)—stands to further the understanding of hemispheric differences in lateralized functions in healthy and disease states.

Anatomical tract-tracing studies in nonhuman primates indicate that "structural" connectivity profiles in frontal corticostriatal circuits are highly lateralized (Goldman 1978; Fallon and Ziegler 1979; Goldman-Rakic 1981). Specifically, frontal cortical regions project predominantly to the ipsilateral striatum with only a limited number of projections crossing the corpus callosum to terminate in the contralateral striatum (Goldman 1978, Fallon and Ziegler 1979, Goldman-Rakic 1981). This suggests that a given striatal area's structural connectivity profile is heavily weighted toward its ipsilateral connections. Yet, prior functional imaging studies find that the striatum's "functional" connections with homotopic areas of the ipsilateral and contralateral frontal cortex appear qualitatively comparable (Postuma and Dagher 2006; Di Martino et al. 2008). The absence of readily apparent laterality in frontal corticostriatal "functional" connections likely arises from the strong cortico-cortical connections and correlated activity between homotopic cortical regions, wherein any third region (e.g., the striatum) would be expected to have similar correlated activity with both regions.

Therefore, although absolute levels of FC profile laterality are likely very low throughout the striatum, the possibility remains that there is meaningful variation—both spatially within the striatum and across individuals. Characterization of this variation in a normative sample would provide a novel basis to probe laterality in frontal corticostriatal circuits in various disease states. Furthermore, identification of laterality "hotspots," where the difference between the ipsilateral and contralateral connectivity profiles is relatively large, may indicate striatal locations that play important roles in lateralized functions. It is also of interest to determine whether left-handedness influences differences in fronto-striatal connectivity profile laterality compared with right-handedness. Given that left-handedness is appreciably more common among a number of neurodevelopmental and neuropsychiatry populations that display atypical fronto-striatal FC (Sommer et al. 2001; Lindell and Hudry 2013), findings in a normative sample may serve as a basis for understanding the relationship between handedness and abnormal fronto-striatal connectivity in these disease states.

Materials and methods

Overview

Here we propose and implement a modified voxel-wise fingerprinting (Mars et al. 2016) approach to quantify the laterality magnitude of each striatal voxel's frontal cortical FC profile. As the foundation for our analytic pipeline, we separately established an ipsilateral and a contralateral frontal cortex connectivity fingerprint for each voxel in the striatum. Each fingerprint encoded the strength of FC between a given striatal voxel and 15 a priori defined unilateral frontal cortical subregions ("targets"). The difference between the ipsilateral and contralateral fingerprint at each voxel—measured via Manhattan distance (Mars et al. 2016)—was operationalized to represent the overall magnitude of laterality in corticostriatal functional connections at each striatal voxel. This allowed for examination of regional variation in FC laterality within the striatum, and the identification of laterality "hotspots." We then compared the Manhattan distance (laterality magnitude) at homotopic voxels in the right and left striatum to examine the degree of FC laterality. Finally, we examined which frontal cortical subregions were the biggest drivers of FC laterality.

We repeated this process in a series of sensitivity and replicability tests. First, we examined replicability in an independent cohort of high-quality, low head-motion subjects. Second, to examine the robustness of the fingerprinting method for assessing laterality magnitude, we examined the effect of using a different cortical atlas parcellation. If the connectivity profile laterality metric is indeed an inherent property of a voxel's connectivity profile and not an artifact of a specific atlas parcellation, we would expect the voxels identified as having comparatively high laterality to remain largely consistent, regardless of the atlas used. As an additional test of methodological robustness, we examined the effect of using different methods for combining data from different scanning sessions. Third, we examined differences between right-handed and left-handed individuals. Finally, we assessed whether connectivity profile laterality magnitude was associated with behavioral performance on tasks that recruit lateralized functions (i.e., inhibition and language) and one that does not (i.e., delay discounting).

Participants

Resting-state data used in these analyses are derived from the Human Connectome Project (HCP) Q1–Q6 Data Release. A detailed description of HCP subject recruitment has been published (Van Essen et al. 2013; Glasser et al. 2016). Briefly, individuals were excluded by the HCP if they reported a history of major psychiatric disorder, neurological disorder, or medical disorder known to influence brain function.

We curated three nonoverlapping samples from this dataset. The first, drawn from (Chen et al. 2016), included subjects who were unrelated and met the following stringent head-motion criteria: 1) range of head motion in any translational direction less than 1 mm and 2) average scan-to-scan head motion less than 0.2 mm. After excluding one subject due to artifacts, this high-quality, low head-motion sample consisted of 77 individuals (age: 22–35, 28 males, all right-handed). Second, we curated a sample of $n = 77$ gender-

Table 1. Sample demographics.

	Discovery sample ($n = 261$)	Low head-motion replication sample ($n = 77$)	Left-handed sample ($n = 77$)
Age (mean ± SD)	28.31 ± 3.90	29.09 ± 3.86	28.75 ± 3.72
Gender (% male)	44.4%	36.4%	50.6%
Edinburgh handedness inventory (mean ± SD)	75.98 ± 21.47	89.68 ± 8.79	−64.68 ± 21.34

and age-matched left-handed individuals to permit evaluations of the relationship between handedness and connection laterality. We used nearest neighbor matching via the R program MatchIt (https://cran.r-project.org/web/packages/MatchIt/MatchIt.pdf) to select the left-handed sample. Briefly, the program computed a distance between each low-motion sample subject and all left-handed HCP subjects, and, one by one, selected a match for each low-motion sample subject. Third, we curated a larger pool of right-handed individuals that included subjects who 1) were not in the $n = 77$ low head-motion dataset, 2) were not related to any subjects in the $n = 77$ low head-motion dataset, 3) were not related to each other, 4) had completed REST1 sessions, and 5) were free from quality-control issues. This larger sample consisted of 269 individuals (eight subjects were later removed for excessive motion, resulting in a final sample of $n = 261$). We used this larger sample as the Discovery sample for all analyses; reproducibility was then assessed using the low head-motion dataset as a Replication sample. Age, gender, and handedness information for each sample is presented in Table 1.

fMRI data acquisition

HCP neuroimaging data were acquired with a standard 32-channel head coil on a Siemens 3 T Skyra modified to achieve a maximum gradient strength of 100 mT/m (Uğurbil et al. 2013; Van Essen et al. 2013; Glasser et al. 2016). Gradient-echo EPI images were acquired with the following parameters: TR = 720 ms, TE = 33.1 ms, flip angle = 52°, FOV = 280 × 180 mm, Matrix = 140 × 90, Echo spacing = 0.58 ms, BW = 2290 Hz/Px. Slice thickness was set to 2.0 mm, 72 slices, 2.0 mm isotropic voxels, with a multiband acceleration factor of 8. Resting-state data were acquired from two runs of approximately 14.4 min each (REST1). Participants were instructed to lie still with their eyes open and fixated on a bright crosshair on a dark background. One run was acquired with a right-to-left phase encoding (REST1_RL) and the other run was acquired with a left-to-right phase encoding (REST1_LR). Thus, REST1 is comprised of 28.8 min of data. REST1_RL and REST1_LR were combined by concatenation of their time series. However, to assess robustness to the method of combining REST1_RL and REST1_LR, we also performed sensitivity analyses in which the FC matrices produced from the REST1_LR and REST1_RL time series were averaged.

Preprocessing

We began with HCP minimally preprocessed resting-state data (Glasser et al. 2013). Briefly, this preprocessing pipeline removes spatial distortions, realigns volumes to compensate for subject motion, registers the echo planar functional data to the structural data, reduces the bias field, normalizes the 4D image to a global mean, and masks the data with a final FreeSurfer-generated brain mask (Glasser et al. 2013) We further preprocessed these scans including spatial blurring with a 6-mm full-width half-maximum Gaussian kernel and temporal filtering ($0.01 < f < 0.1$ Hz).

ROIs for the striatal fingerprint were based on the frontal cortical parcellation definitions from the Harvard-Oxford cortical atlas (Supplementary Fig. 1) and included supplementary motor cortex, superior frontal gyrus, subcallosal cortex, precentral gyrus, paracingulate gyrus, middle frontal gyrus, insular cortex, inferior frontal gyrus pars opercularis, inferior frontal gyrus pars triangularis, frontal pole, frontal orbital cortex, frontal operculum cortex, frontal medial cortex, central opercular cortex, and anterior cingulate cortex. Sample-specific right and left striatum masks were created by averaging the union of the caudate, putamen, and nucleus accumbens FreeSurfer parcellations of each subject.

Resting-state functional connectivity (rsFC) was assessed for each frontal cortical seed ROI using the mean resting-state BOLD time series, extracted from each participant. The mean time series from each ROI was included in a GLM with 17 additional regressors of no interest: six motion parameters (three translations and three rotations) obtained from the rigid-body alignment of EPI volumes and their six temporal derivatives; the mean time series extracted from white matter; the mean times series extracted from CSF; and a second-order polynomial to model baseline signal and slow drift. To further control for subject motion, volumes were censored for framewise motion displacement (i.e., volume-to-volume movement) >0.5 mm (Power et al. 2012; Yan et al. 2013). The outputs of R values from the GLM were converted to Z-scores using the Fisher R-to-Z transform.

Behavioral tasks

To study the relationship between connectivity profile laterality and behavior, we examined 1) a task that

engages a lateralized functional capacity primarily in the left hemisphere (i.e., language), 2) a task that engages a lateralized functional capacity primarily in the right hemisphere (i.e., inhibition), and 3) a task that engages a nonlateralized functional capacity (i.e., delay discounting). For language, we examined data from the NIH toolbox's (Weintraub et al. 2013) picture vocabulary task in which subjects were presented with four pictures and an audio recording of a word and were asked to select the picture that most closely matches the meaning of the word [PicVocab] (Gershon et al. 2014). Distractor pictures included those that were phonologically similar, semantically similar, visually similar, and/or represented common misconceptions of a word's meaning. This task measures auditory comprehension and vocabulary knowledge, and the performance metric was based on accuracy. For inhibition, we examined data from the NIH toolbox's flanker task (Zelazo et al. 2014), which also engages attention. In this task, subjects were asked to focus on a centrally presented stimulus and report its left–right orientation while inhibiting attention to other stimuli (arrows) flanking it. Sometimes the central stimulus pointed in the same direction as the "flankers" (congruent) and sometimes in the opposite direction (incongruent). Scoring is based on a combination of accuracy and reaction time. Lastly, for the nonlateralized capacity task, we examined findings from a delay discounting task (Estle et al. 2006) that measures the magnitude by which subjects undervalue rewards that are delayed in time (a property often referred to as cognitive impulsivity). For this task, the examined outcome measures were area under the curve for discounting of $200 [DDisc_AUC_200] and area under the curve for discounting of $40 000 [DDisc_AUC_40K] (Myerson et al. 2001).

Analytic strategy

Comparison of ipsilateral and contralateral fingerprints within striatal voxels

In order to compare the ipsilateral and contralateral frontal cortical connectivity fingerprint at each voxel in the striatum, we carried out the following procedure (Supplementary Fig. 2). First, for each subject, we generated voxel-wise maps of the correlation (Pearson's *r*) between the mean time series of each frontal cortical ROI and each voxel in the striatum. These Pearson's *r* maps were transformed to Z-score maps using Fisher's *r*-to-Z transformation. This resulted in 30 voxel-wise Z-score striatal maps (15 each for the ipsilateral and contralateral hemisphere cortical ROIs). Then, we computed voxel-wise Z-score difference maps by taking the absolute value of the difference between the ipsilateral and contralateral Z-score map of each ROI:

$$|\mathrm{RH_Z} - \mathrm{LH_Z}|_{\mathrm{ROI}}$$

This produced 15 difference maps (one for each ipsilateral–contralateral ROI pair) for each subject. Next, we took the sum of the 15 difference maps, resulting in a final voxel-wise map for each subject whose values represent the Manhattan distance between the ipsilateral and contralateral frontal cortical fingerprint at each striatal voxel:

$$|\mathrm{RH_Z} - \mathrm{LH_Z}|_{\mathrm{frontal\ orbital}} + |\mathrm{RH_Z} - \mathrm{LH_Z}|_{\mathrm{frontal\ medial}} + \cdots + |\mathrm{RH_Z} - \mathrm{LH_Z}|_{\mathrm{insula}} = \sum_{i=1}^{15} |\mathrm{RH_Z} - \mathrm{LH_Z}|_i$$

In this way, the Manhattan distance value provides a measure of the magnitude of total frontal cortical FC laterality at each striatal voxel. Finally, we computed the mean of the cohort's subject-level Manhattan distance maps, resulting in a group-level voxel-wise map encoding the average within-subject Manhattan distance at each striatal voxel.

Typically, in order to determine a significance threshold for Manhattan distance values derived for fingerprinting analysis, the fingerprints are permuted 10 000 times or more to create a Manhattan distance test statistic distribution (Mars et al. 2016). This kind of analysis informs whether any of the empirically measured Manhattan distance values are significantly bigger (or smaller) than would be expected by chance if the data were random. However, this kind of analysis would be uninformative for the purposes of this investigation. As discussed previously, due to the highly correlated activity of homotopic frontal cortical ROIs, any third region (e.g., a striatal voxel) will have a very similar magnitude of connectivity with the LH and RH ROI of a region. As a corollary then, a striatal voxel's connectivity with a given region's LH ROI is likely to be more similar to its connectivity with that same region's RH ROI than the RH ROI of any other region. The result is that a Manhattan distance calculated by summing the connectivity differences between pairs of matched LH-RH ROIs (e.g., right OFC—left OFC), as opposed to mismatched LH-RH ROIs (e.g., right OFC—left dlPFC), will almost always yield the lowest or close to the lowest possible Manhattan distance value. Since the permutation testing process involves the calculation of Manhattan distances from randomly permuted LH-RH ROI pairs, a priori we know that voxels' empirically measured Manhattan distances will be significantly smaller than nearly all possible values produced from random permutation. As a result, the permutation approach would simply reconfirm that overall laterality in frontal corticostriatal circuits is substantially lower than what it could be theoretically. Therefore, we do not use the permutation approach and instead take an alternative approach to thresholding (described below) that is more aligned with the focus of this investigation.

Our question of interest is whether any of the empirically observed Manhattan distance values in the striatum is substantively greater than the rest, within the neurobiologically realized range of laterality. To examine this question, we tested for the presence of outliers

in the voxel-wise distribution of Manhattan distance values. To establish an outlier threshold, we used the interquartile range (IQR) criterion (Barbato et al. 2011), defined as values above the sum of the distribution's third quartile and 1.5 multiplied by the interquartile range (i.e., $>q_{.75} + [1.5*\text{IQR}]$). These threshold values were determined to be Manhattan distance >1.027 for the right striatum, and Manhattan distance >1.013 for the left striatum. Voxels whose Manhattan distance was so classified as an outlier were labeled as "high laterality" (HL) voxels, and clusters of HL voxels were considered to constitute "laterality hotspots."

Laterality directionality

The Manhattan distance calculation, with its inclusion of absolute value terms, obscures whether overall connectivity laterality is stronger in the direction of the right or left frontal cortex. We therefore conducted an additional "directionality analysis" by repeating the above steps with an altered Manhattan distance calculation that excludes the absolute value computations:

$$\begin{aligned}&RH_Z - LH_{Z\ \text{frontal orbital}} + RH_Z - LH_{Z\ \text{frontal medial}} + \dots \\ &+RH_Z - LH_{Z\ \text{insula}} = \sum_{i=1}^{15} RH_Z - LH_{Z\ i}\end{aligned}$$

This additional voxel-wise map was used to determine the direction of laterality at hotspots identified in the initial Manhattan distance analysis.

Comparison of laterality in homotopic striatal areas

To compare the magnitude of laterality in homotopic areas of the right and left striatum in a voxel-wise manner, we carried out the following procedure. First, in order to establish geometrical homotopy between the right and left striatum, we created subject-level symmetrical templates. Specifically, for each subject, we registered flipped (using AFNI's (Cox 1996) 3dLRflip program) and unflipped T1w images to one another using half-transformations (produced by nonlinear warping via AFNI's 3dQwarp program) so as not to bias the transformation matrix by one hemisphere or the other. We then applied the half-transformation matrices to the subject's right and left striatal Manhattan distance maps (using nearest-neighbor interpolation via AFNI's 3dNwarpApply program), thereby creating symmetrical Manhattan distance maps. The absolute values of the difference of these symmetrical Manhattan distance maps were then taken to compute the Manhattan distance difference map—measuring the difference in laterality magnitude between homotopic areas of the right and left striatum. Finally, nonzero voxels were average across all subjects to create a group-level Manhattan distance difference map.

Here, we again tested for the presence of HL voxels to identify voxels whose Manhattan distance difference was substantively different than the rest. The IQR threshold for this analysis was determined to be Manhattan distance difference > 0.439. To further corroborate findings, we conducted a paired *t*-test by comparing, in a voxel-wise manner, each subject's right Manhattan distance heatmap to their left striatum Manhattan distance heatmap. This analysis examined the statistical significance of the average within-subject Manhattan distance difference at each homotopic voxel pair. We used a voxel-level threshold of $P < 0.001$ with 3dClustSim (AFNI 20.1.14) to determine a $P < 0.05$ family-wise corrected cluster-level threshold, corresponding to k > 6.

Identification of frontal cortical ROIs driving laterality at hotspots

At each striatal hotspot's peak Manhattan distance coordinates, we examined the absolute value of the difference between the Z-scores for each right hemisphere–left hemisphere ROI pair. These difference values measure the magnitude of laterality for each ROI pair. In order to determine the ROI pairs most strongly contributing to laterality at each hotspot, we identified ROI pairs whose $|RH_Z - LH_Z|$ value constituted an outlier in the distribution of all ROI $|RH_Z - LH_Z|$ values throughout the striatum. This threshold was $|LH_Z - RH_Z| > 0.068$ for the right and left striatum.

Sample replication analysis

To examine replicability, we repeated the above analyses in the high-quality, low head-motion $n = 77$ Replication group. To evaluate the spatial correspondence between laterality hotspot voxels identified in the initial Discovery sample and those identified by the Replication sample, we performed a Dice coefficient analysis. To do so, we first calculated the Dice coefficient (Dice 1945) between corresponding laterality hotspot voxel clusters, defined as

$$\frac{2\,|\,X \cap Y\,|}{|\,X\,| + |\,Y\,|}$$

where $|X \cap Y|$ is the number of voxels where cluster X and cluster Y overlap, $|X|$ is the total number of voxels in cluster X, and $|Y|$ is the total number of voxels in cluster Y. Then, to determine a significance threshold, we performed permutation testing. Using the recently developed BrainSMASH (Burt et al. 2020) program to create permuted null brain maps that preserve spatial autocorrelation, on each of 10 000 iterations, the voxel locations of cluster Y were randomized throughout the striatal mask, and a Dice coefficient between cluster X and the spatially randomized cluster Y was calculated. This created a Dice coefficient test statistic distribution customized to the striatal mask space. Clusters were considered to have significant spatial overlap if their Dice coefficient corresponded to $P < 0.05$.

Atlas sensitivity analysis

In order to ensure that laterality results were not an artifact of the specific atlas cortical parcellation schema chosen and were robust across parcellation definitions,

we repeated the above analyses using the atlas of intrinsic connectivity of homotopic areas (AICHA) (Joliot et al. 2015)—which is parcellated into 59 frontal cortical ROIs per hemisphere—and evaluated spatial correspondence (again using Dice coefficient analysis and permutation testing) of identified HL voxels with HL voxels identified using the Harvard-Oxford atlas. If the connectivity profile laterality metric is indeed an inherent property of a voxel's connectivity profile and not an artifact of a specific atlas parcellation, we would expect the voxels identified as having comparatively high laterality to remain largely consistent, regardless of the atlas used. This follows from how the Manhattan distance is calculated.

The Manhattan distance calculation involves a summing over all right-hemisphere/left-hemisphere ROI-pair differences in an atlas. The input data to the Manhattan distance calculation, therefore, is sampled from the full space of the atlas (i.e., data from all voxels in right frontal cortex and all voxels in left frontal cortex are included). If two atlases cover roughly the same underlying space (e.g., right and left frontal cortex), then using either atlas for a Manhattan distance calculation will include data from roughly the same space. This is because regardless of how the ROIs are parcellated on top of that space, the ROI-pair differences are summed back together at the end of the calculation. Thus, while a voxel's Manhattan distance value itself would differ in different atlas parcellations, its relative magnitude compared with other voxels should remain consistent.

Laterality in right-handed versus left-handed individuals

Since all subjects in the Discovery and Replication samples were right-handed, we also repeated the analysis in an additional sample consisting only of left-handed individuals from the HCP. Similar laterality magnitude maps in right-handed and left-handed individuals would suggest that, regardless of which hemisphere is dominant, the magnitude of the hemispheric dominance in homotopic striatal areas is similar.

Here, we performed a voxel-wise two-sample *t*-test to assess laterality magnitude differences between these left-handed and the right-handed individuals from the Replication sample. Additionally, we performed supervised classification using a support vector machine (SVM) with MATLAB's Statistics and Machine Learning Toolbox (version 2020b) to examine whether the voxel-wise Manhattan distance (i.e., laterality magnitude) maps could be used to distinguish between the right-handed and left-handed individuals. To avoid data leakage and overfitting, we used nested 10-fold cross-validation to estimate an unbiased generalization performance. First, the dataset was randomly divided into 10 folds of approximately 15 subjects each. Then, for each of 10 iterations, one of the 10 folds was left out for testing, while the other 9-folds were used for model training. On each iteration, an outer loop performed dimensionality reduction via feature selection on the training set by selecting the most predictive features (i.e., voxels), as determined via F-tests, for model training (Mwangi et al. 2014). We examined different levels of feature selection to assess robustness to this parameter (i.e., 5%, 10%, 25%, 33%, 50%, 66%, 75%, and 100% of the most predictive voxels determined via *F*-tests). Then, for hyperparameter optimization and model selection, an inner loop performed Bayesian optimization with 10-fold cross-validation on the training set using the selected features. Optimization selected a linear kernel with box constraint hypermeter $C = 0.0018$. Lastly, the optimized model was used to predict the handedness of the subjects in the left-out fold. The final metric of interest was the mean accuracy of test predictions across each of the 10 iterations.

Laterality and behavior

To examine whether voxel-wise laterality magnitude was associated with performance on tasks engaging lateralized functional capacities, we conducted two types of analyses. First, we performed traditional, univariate voxel-wise regressions to assess whether the laterality magnitude of individual voxels was correlated with task performance. For laterality magnitude, we used the non-absolute Manhattan distance values in order to examine directionality (i.e., rightward or leftward dominated laterality). We used the age-adjusted scores for each of the three tasks and controlled for gender in each analysis. We used a voxel-level threshold of $P < 0.001$ with 3dClustSim (AFNI 20.1.14) to determine a $P < 0.05$ family-wise corrected cluster-level threshold, corresponding to $k > 6$.

Second, we performed supervised support vector regression (SVR) to examine whether voxel-wise laterality magnitude maps could predict task performance. The model was trained on the Discovery sample, and then tested on the Replication sample. We examined different levels of feature selection to assess robustness to this parameter (i.e., 5%, 10%, 25%, 33%, 50%, 66%, 75%, and 100% of the most predictive voxels determined via *F*-tests). We then used Bayesian optimization with 10-fold cross-validation to optimize hyperparameters. The optimized model trained to take the identified set of voxels as input was then used to predict the behavioral performance of subjects in the Replication sample. The outcome metric of interest was the correlation between actual and predicted performance.

Results

Comparison of ipsilateral and contralateral frontal cortex fingerprints within the striatum

We identified several laterality "hotspots" indicative of comparatively high "dissimilarity" between ipsilateral and contralateral frontal corticostriatal connectivity profiles. Laterality magnitude heatmaps illustrate peaks in the left rostral central caudate, the right rostral ventral

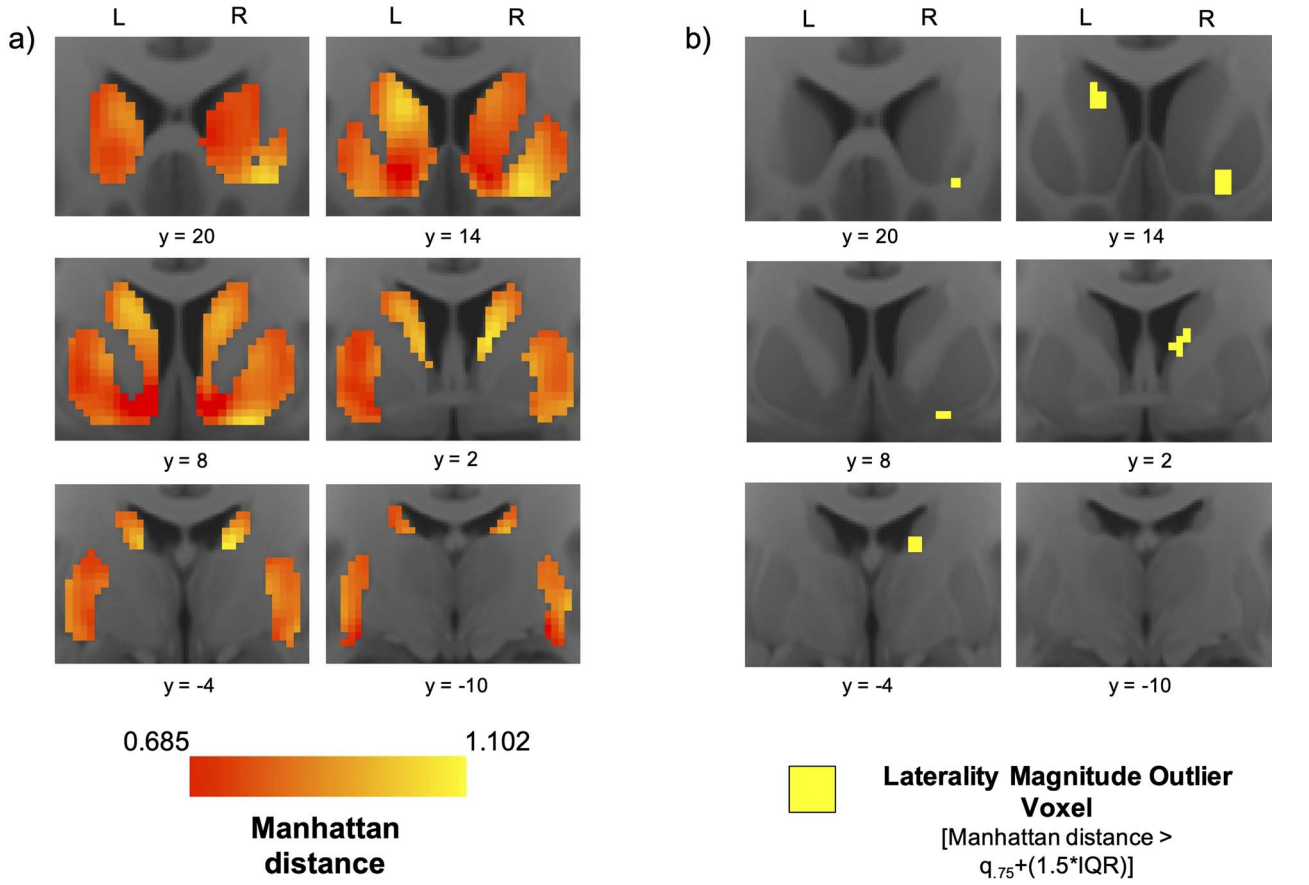

Fig. 1. Functional connectivity profile laterality: heatmaps and hotspots. (*a*) Average voxel-wise heatmaps of Manhattan distance in the left and right striatum from the $n = 261$ Discovery dataset. Warm colors indicate larger difference between a voxel's ipsilateral and contralateral frontal cortical connectivity profile. (*b*) Maps highlighting laterality "hotspot" voxels whose Manhattan distance constitutes an extreme (outlier) in the distribution.

putamen, and the right caudal ventral caudate (Fig. 1*a*). In the right striatum, a cluster of 17 HL voxels was identified in the rostral ventral putamen (Fig. 1*b*).

At the peak Manhattan distance voxel of this right rostral ventral putamen cluster, the $|RH_Z - LH_Z|$ laterality of six ROI pairs surpassed the outlier threshold (Table 2). Furthermore, the directionality analysis showed that the right rostral ventral putamen hotspot had the most right-lateralized frontal cortical connectivity anywhere in the bilateral striatum (Supplementary Fig. 3). A cluster of 27 HL voxels was also identified in the right caudal ventral caudate, where the $|RH_Z - LH_Z|$ laterality of seven ROI pairs surpassed the HL threshold (Table 2). In the left striatum, a cluster of 20 HL voxels was identified in the rostral central caudate (Fig. 1*b*). At the peak Manhattan distance voxel of this rostral central caudate cluster, the $|RH_Z - LH_Z|$ laterality of nine ROI pairs surpassed the HL threshold (Table 2). Furthermore, the directionality analysis showed that this rostral central caudate hotspot had the most left-lateralized frontal cortical connectivity of anywhere in the bilateral striatum (Supplementary Fig. 3). The pars opercularis was the only cortical ROI among the top three most lateralized ROIs at all three hotspots.

Pars opercularis laterality

Given observations of strong connectivity laterality with the pars opercularis at each of the striatal laterality hotspots, we mapped the voxel-wise laterality of pars opercularis connectivity throughout the striatum to visualize the complete spatial distribution of its magnitude (Fig. 2). For this mapping, we used $RH_Z - LH_Z$ rather than $|RH_Z - LH_Z|$ in order to distinguish between striatal areas with RH versus LH pars opercularis-dominated laterality. We also examined ROI-specific HL voxels (IQR threshold: $RH_Z - LH_Z > \pm 0.068$).

In the right striatum, RH pars opercularis-dominated laterality peaked in the rostral ventral putamen, where a cluster of 34 HL voxels was identified. A cluster of 12 RH-dominated HL voxels was also identified in the right caudal putamen, and one RH-dominated HL voxel was identified in the right caudal ventral caudate. There were no instances of LH pars opercularis-dominated HL voxels in the right striatum. In the left striatum, LH pars opercularis-dominated laterality peaked in the rostral central caudate, where a cluster of 72 HL voxels was identified. No HL voxels were identified elsewhere in the left striatum. There were no instances of RH pars opercularis-dominated HL voxels in the left striatum.

Table 2. Frontal cortical drivers of laterality.

Frontal cortical ROI	Connectivity laterality $\|LH_Z - RH_Z\|$	Connectivity laterality $\|LH_Z - RH_Z\|$	Connectivity laterality $\|LH_Z - RH_Z\|$
Frontal orbital	**0.182**	**0.092**	**0.096**
Subcallosal cortex	**0.093**	**0.069**	**0.079**
Pars opercularis	**0.096**	**0.119**	**0.103**
Pars triangularis	**0.111**	**0.094**	**0.110**
Frontal pole	**0.070**	**0.081**	**0.079**
Middle frontal gyrus	0.061	**0.091**	**0.076**
Superior frontal gyrus	0.059	0.067	**0.099**
Frontal operculum	**0.068**	**0.100**	**0.069**
Frontal medial	0.059	0.053	0.057
Insula	0.059	0.059	0.066
Paracingulate gyrus	0.046	0.047	**0.077**
Supplementary motor	0.037	0.046	0.047
Central operculum	0.043	0.044	0.059
Precentral gyrus	0.037	0.044	0.047
ACC	0.035	0.040	0.039

Table 2: Bolding indicates that an ROI's $|LH_Z - RH_Z|$ value at the hotspot peak coordinate surpassed the striatum-wide $|LH_Z - RH_Z|$ outlier threshold ($|LH_Z - RH_Z| > 0.068$).

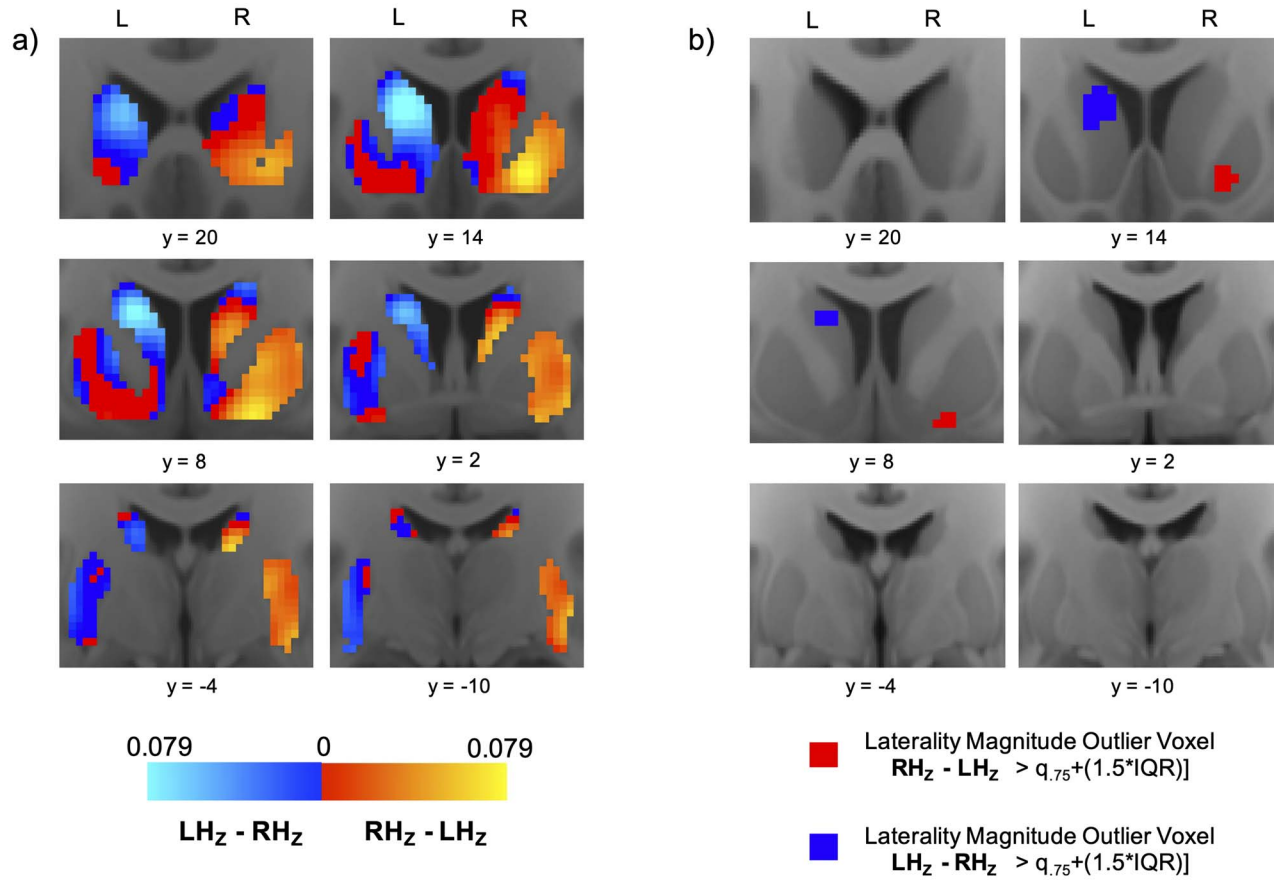

Fig. 2. Pars opercularis connectivity laterality: heatmaps and hotspots. (*a*) Average voxel-wise heatmaps of laterality in pars opercularis functional connectivity in the left and right striatum. Warm spectrum colors indicate voxels whose connectivity with right pars opercularis is stronger than their connectivity with left pars opercularis. Cooler spectrum colors indicate voxels whose connectivity with left pars opercularis is stronger than their connectivity with right pars opercularis. Brighter hues on each spectrum denote higher levels of laterality. (*b*) Maps highlighting laterality "hotspot" voxels where the difference between connectivity with left and right pars opercularis constitutes an extreme (outlier) in the distribution.

Comparison of laterality magnitude in homotopic areas of the right and left striatum

The Manhattan distance difference heatmap illustrates peaks in the central caudate and ventral putamen (Fig. 3*a*). HL difference voxels were identified in the caudal ventral caudate and caudal ventral putamen (Fig. 3*b*). Furthermore, the paired samples *t*-test revealed that 1) laterality magnitude was significantly greater in the left striatum than in the right striatum in a cluster of size $k = 52$ with peak coordinate at (−12, 20, 6) in

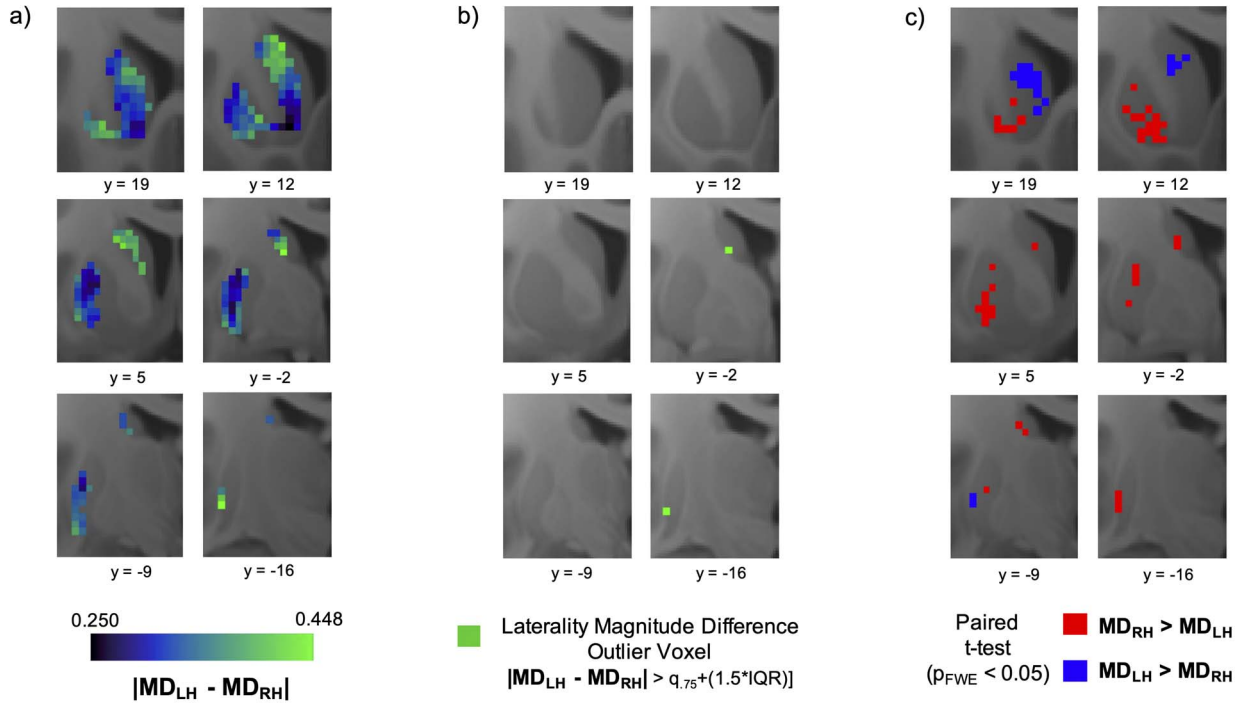

Fig. 3. Laterality magnitude difference in homotopic striatal voxels. (*a*) Voxel-wise heatmaps of Manhattan distance difference values. The value at each voxel represents the subject average difference in connectivity profile laterality between the voxel and its homotopic pair in the contralateral striatum. Greener colors indicate higher levels of Manhattan distance difference, and bluer colors indicate lower levels. (*b*) Maps highlighting laterality difference "hotspot" voxels where the difference in laterality between the right and left striatum constitutes an extreme (outlier) in the distribution. (*c*) Statistically significant clusters from paired *t*-test. Red clusters indicate areas where right striatum laterality magnitude was significantly larger than left striatum laterality magnitude; blue clusters indicate areas where left striatum laterality magnitude was significantly larger than right striatum laterality magnitude.

the rostral caudate; and 2) laterality magnitude was significantly greater in the right striatum than in the left striatum in a cluster of size $k = 147$ with peak coordinate at (24, 2, 4) in the caudal putamen (Fig. 3*c*).

Sensitivity and replication analyses

Replication analysis

The identified HL voxels in the low head-motion $n = 77$ Replication sample had significant spatial correspondence to those identified in the $n = 261$ Discovery sample in the right striatum (Dice coefficient = 0.207, $P < 0.0001$) and left striatum (Dice coefficient = 0.158, $P < 0.0001$), with overlap present in the right caudal ventral caudate and left rostral central caudate (Fig. 4*a*,*b*).

Atlas sensitivity analysis

In the atlas sensitivity analysis, identified HL voxels using the AICHA atlas had significant spatial correspondence to those identified using the Harvard-Oxford atlas in both the right striatum (Dice coefficient = 0.628, $P < 0.0001$) and left striatum (Dice coefficient = 0.250, $P < 0.0001$), with overlap present in bilateral caudal ventral caudate (Fig. 4*a*,*c*).

Preprocessing sensitivity analysis

Identified HL voxels using concatenated REST1_RL and REST1_LR time series had significant spatial overlap to those identified using averaged REST1_RL and REST1_LR FC matrices in both the right striatum (Dice coefficient = 0.450, $P < 0.0001$) and left striatum (Dice coefficient = 0.280, $P < 0.0001$), with overlap present in left rostral caudate and bilateral caudal ventral caudate (Fig. 4*a*,*d*).

As a culmination of these replication and sensitivity analyses, we present the average Manhattan distance map (Supplementary Fig. 4) computed from all eight combinations of sample (Discovery; Replication) atlas (Harvard-Oxford; AICHA) and scan session combination methodology (concatenated time series; averaged FC matrices). This map shows the same laterality magnitude peaks as in the initially identified hotspot locations (i.e., left rostral caudate, right ventral putamen, and bilateral caudal ventral caudate). Coupled with the observation that all maps were highly correlated with one another (all $Rs > 0.7$; Supplementary Table 1), these findings demonstrate that our laterality magnitude measure and the findings derived from it are both robust and reproducible.

Corroborating HL voxel cluster similarities

The small size of the HL voxel clusters thresholded using the IQR outlier criterion led to small Dice coefficient values, despite qualitative evidence of high spatial similarity of corresponding clusters between groups (Fig. 4). To further corroborate this similarity quantitatively, we thresholded the clusters at less stringent values,

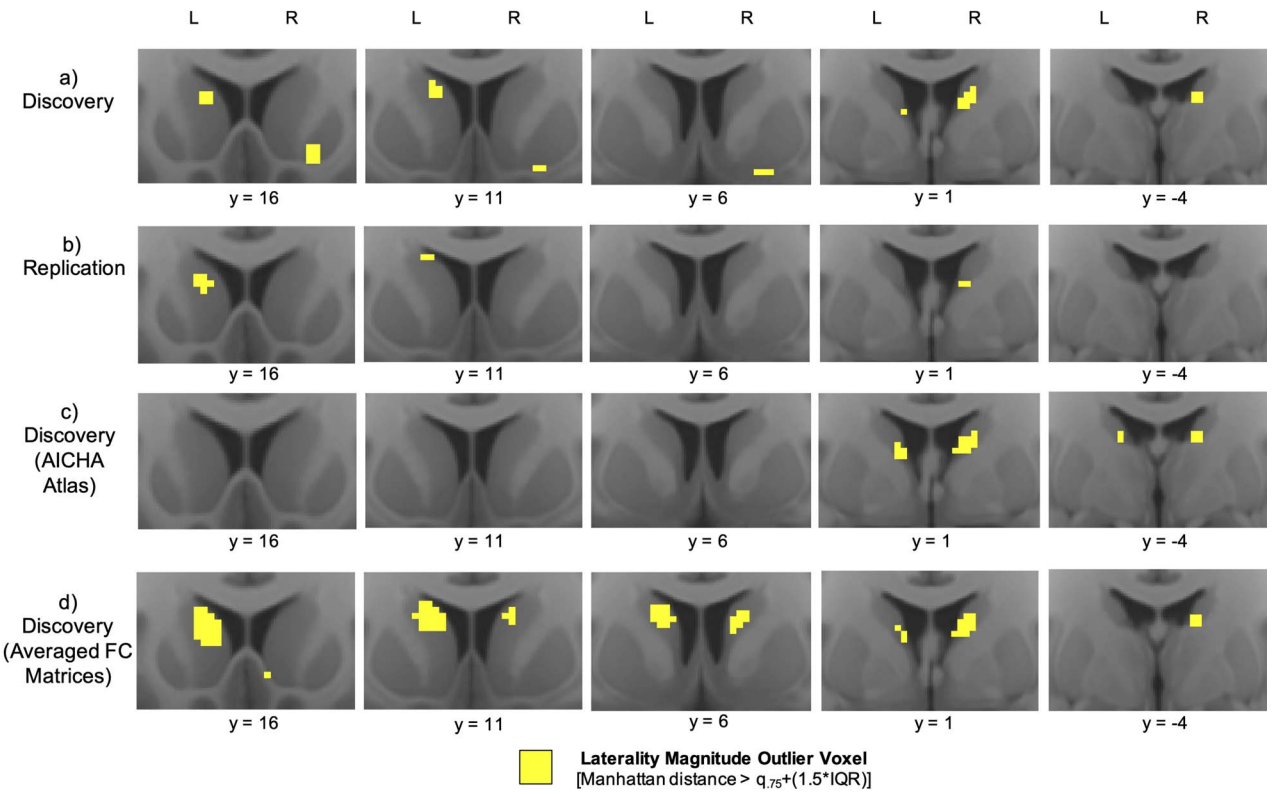

Fig. 4. Replication and sensitivity analyses. Comparing laterality "hotspot" outlier voxels from (*a*) the Discovery sample, to those from (*b*) the Replication sample, (*c*) the Discovery sample using the AICHA atlas instead of the Harvard-Oxford atlas, and (*d*) the Discovery sample using averaged FC matrices instead of concatenated time series.

recalculated Dice coefficients (Supplementary Table 2), and constructed receiver-operating characteristic (ROC) curves by varying the threshold to assess area under the curve (AUC) (Supplementary Fig. 5). The additional threshold values used were the maximum value, third quartile, median, first quartile, and minimum value of each group's voxel-wise Manhattan distance distribution. High Dice coefficient values were observed for the less stringent thresholds (Supplementary Table 2).

tSNR

Striatal voxels' tSNR and Manhattan distance (laterality magnitude) values were weakly correlated across both hemispheres, as computed using either concatenated time series ($r = 0.024$, $P = 0.165$ [Harvard-Oxford]; $r = 0.133$, $P < 0.001$ [AICHA]) or averaged connectivity matrices ($r = 0.086$, $P < 0.001$ [Harvard-Oxford]; $r = 0.094$, $P < 0.001$ [AICHA]), indicating that spatial variation in tSNR across the striatum was negligibly related to spatial variation in connectivity profile laterality magnitude.

Left-Handed replication sample

As in the right-handed Discovery and Replication samples, HL voxels were identified in the left-handed cohort in bilateral caudal ventral caudate (Supplementary Fig. 6*a*). However, HL voxels were not identified in the right ventral putamen or left rostral caudate, and therefore spatial correspondence of HL voxels was not significant for either the right striatum (Dice coefficient = 0.041, $P < 0.206$) or left striatum (Dice coefficient = 0, $P = 1$). Nonetheless, unthresholded heatmaps were significantly correlated (right striatum: $R = 0.620$, $P < 0.0001$; left striatum: $R = 0.600$, $P < 0.0001$) and qualitatively similar (Supplementary Fig. 6*b*,*c*) to the right-handed samples, with laterality magnitude peaks visible in the hotspot locations identified in the right-handed samples (i.e., right ventral putamen, left rostral caudate, and bilateral caudal ventral putamen). Furthermore, the two-sample *t*-test did not reveal any significant voxel-wise group differences between the right-handed and left-handed groups, and the machine learning classifier trained on the heatmaps was not able to distinguish between the two groups above chance level (accuracy did not exceed 53.9% at any level of feature selection).

Laterality magnitude and behavior

Univariate voxel-wise analyses

Higher scores on the PicVocab language task were associated with greater leftward laterality magnitude in a cluster of size $k = 30$ with peak coordinate (−8, 16, 0) in the left rostral caudate (Fig. 5). The superior segment of this cluster adjoined the laterality hotspot identified in the left rostral caudate. Higher scores on the Flanker inhibition/attention task were associated with greater rightward laterality magnitude in a cluster of size $k = 17$ with peak coordinate (16, 6, −10) in the right ventral

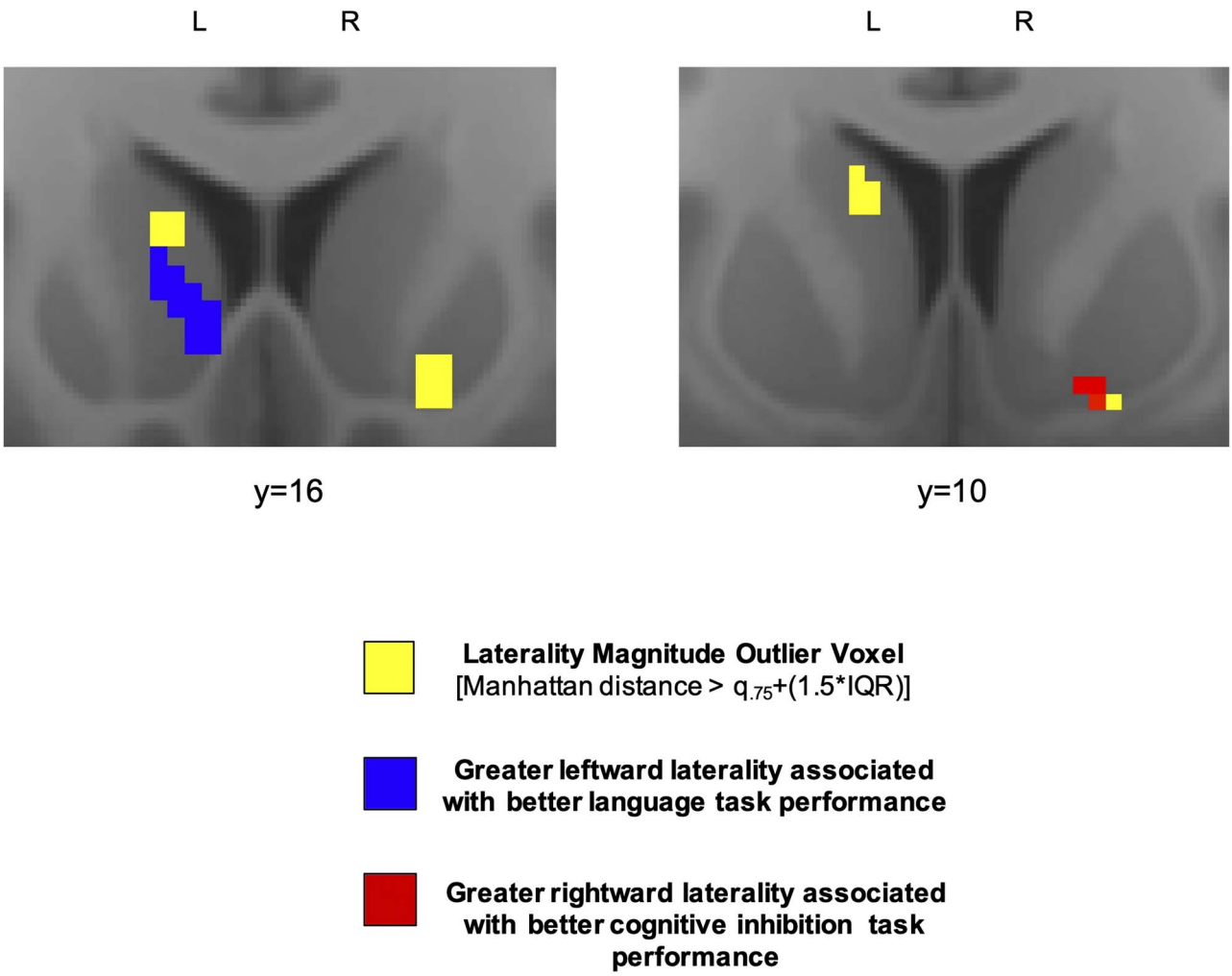

Fig. 5. Connectional laterality and lateralized functions. Relationship between laterality magnitude and performance on tasks engaging lateralized capacities. Maps display proximity of significant clusters (red and blue) to separately identified high laterality voxels (yellow).

putamen (Fig. 5). Three voxels in this cluster overlapped with the laterality hotspot identified in the right ventral putamen. Higher scores on the Flanker inhibition/attention task were also associated with greater rightward laterality magnitude in a cluster of size $k = 17$ with peak coordinate (24, 0, 4) in the right caudal dorsal putamen. No relationships were found between laterality magnitude and performance on the nonlateralized delay-discounting task.

The machine learning approach was unsuccessful at using multivariate laterality magnitude heatmaps to significantly predict out-of-group performance on any of the tasks across a wide range of examined feature selection values (i.e., 5%, 10%, 25%, 33%, 50%, 75%, and 100% of voxels).

Discussion

Functional connectivity profile laterality has been shown to be very low throughout the human striatum (Postuma and Dagher 2006; Di Martino et al. 2008). However, we find that the spatial distribution of laterality magnitude is nonhomogeneous, as a handful of focal striatal areas display connectivity profiles that are substantively more lateralized than the rest of the striatum. These striatal "laterality hotspots" include the right ventral putamen, the left rostral central caudate, and the bilateral caudal ventral caudate. Furthermore, interindividual variance in laterality magnitude at these hotspots was associated with performance on tasks engaging lateralized functional capacities, but not with performance on a task engaging a nonlateralized functional capacity.

The robustness, reproducibility, and spatial specificity of these hotspots were corroborated across several sensitivity and replication analyses. In particular, we demonstrated that findings remained consistent across different samples, different cortical atlas parcellations, and different rsFC preprocessing choices. Some variability was observed in the presence/absence of HL voxels (those whose laterality magnitude surpassed the IQR threshold) (Fig. 4). This appears attributable to differences in the spreads and shapes of each map's distribution of Manhattan distance values, given that the IQR threshold is derived uniquely for each map based on the properties of its distribution. For example, averaging the FC matrices (Fig. 4*d*) seems to amplify the magnitude of values at the

top of the distribution relative to values between quartiles one and three—resulting in more value surpassing the IQR threshold. Even so, the Dice coefficient analysis demonstrated that spatial overlap of HL voxels across maps was significant.

Furthermore, the high level of correlation between the unthresholded maps (all $Rs > 0.7$) provides confidence that the overall spatial distributions of laterality magnitude were highly similar. As such, these findings provide a robust, normative basis for future comparison with connectivity profile laterality in clinical samples.

Compared with the rest of the striatum, the identified striatal laterality hotspots appear to receive the most dissimilar information from the right and left frontal cortices, which may underlie their role in lateralized brain functions such as response inhibition and language. The direction of lateralization at each hotspot favored the ipsilateral frontal cortex, consistent with the general organization observed in structural corticostriatal connectivity (Shepherd 2013). It is notable that one of the largest sources of connectivity laterality at all of the laterality hotspots was the pars opercularis of the inferior frontal gyrus (BA44), itself a cortical region with well-established lateralized functionality as discussed below (Cantalupo and Hopkins 2001; Hampshire et al. 2010).

In most right-handed (~95%) and left-handed (~75%) individuals (Knecht et al. 2000; Szaflarski et al. 2002), BA44 in the left hemisphere, but not the right hemisphere, is part of Broca's language area (Anwander et al. 2007; Fadiga et al. 2009). The observation that $BA44_{LH}$–$BA44_{RH}$ connectivity laterality peaks in the left central caudate suggests a particular role for this striatal area in language functions. Indeed, the left central caudate has been repeatedly implicated in several aspects of language including language acquisition (Tan et al. 2011), word-finding and the selection of appropriate lexical–semantic responses (Robles et al. 2005), and monitoring and controlling the language currently in use in bilingual speakers (Crinion et al. 2006). The comparatively lower $BA44_{LH}$–$BA44_{RH}$ connectivity laterality in the homotopic right central caudate may reflect the more dominant role of the left central caudate in language processes. Here, we further demonstrate that in the left, but not the right, central caudate, higher levels of LH-lateralized frontal cortical connectivity are associated with stronger performance on a language task.

On the other hand, BA44 in the right hemisphere is strongly implicated in motor inhibition processes (Garavan et al. 1999; Aron et al. 2014). The observation that $BA44_{RH}$–$BA44_{LH}$ connectivity laterality peaks in the right ventrolateral putamen may reflect a particular role for this striatal area in cognitive–motor inhibition. This is consistent with a number of studies that find concurrent activation of right BA44 and right ventrolateral putamen during performance of response inhibition tasks (Garavan et al. 1999; Simmonds et al. 2008; Zandbelt and Vink 2010; Majid et al. 2013; Schel et al. 2014; Jahanshahi et al. 2015) facilitated by BA44's strong neuroanatomical innervation of this striatal area (Korponay et al. 2020). However, these studies also show involvement of the left ventrolateral putamen, which we also find has stronger FC with right BA44 than left BA44. Overall, these findings suggest bilateral involvement of ventrolateral putamen in action inhibition might be related to outsized FC with right BA44. Moreover, we further demonstrate here that in the right ventral putamen higher levels of RH-lateralized frontal cortical connectivity are associated with stronger performance on the cognitive control/inhibition-engaging flanker task.

Interestingly, connectivity profile laterality magnitude did not differ significantly between left-handed and right-handed individuals for any striatal voxels, and a machine learning classifier was not able to use striatum-wide laterality heatmaps to distinguish handedness above chance level. As in the right-handed groups, the left-handed group displayed HL voxels in the bilateral caudal ventral caudate. And while voxels in the right rostral ventral putamen and left rostral central caudate did not surpass the HL threshold in the left-handed group, voxels in these areas displayed comparable levels of laterality to those in the right-handed groups (Supplementary Fig. 6). Furthermore, laterality maps for the right-handed and left-handed groups were strongly correlated (Supplementary Table 1). Overall, these findings suggest that, regardless of differences in intrinsic hemispheric dominance, the degree to which ipsilateral–contralateral frontal cortical connectivity differs at corresponding striatal loci is similar regardless of handedness.

In sum, we find that meaningful and behaviorally relevant variation in FC profile laterality—both spatially within the striatum and across subjects—is evident in corticostriatal circuits. The elucidation of striatal laterality "hotspots," their frontal cortical drivers, and their associations with lateralized functions warrants further examination of these sites in psychiatric illness.

Supplementary material

Supplementary material can be found at *Cerebral Cortex* online.

Funding

National Institute on Drug Abuse (1F32DA048580-01A1 to C.K.); the Intramural Research Program of the National Institute on Drug Abuse (to T.R. and E.A.S.).

Notes

Data were provided by the Human Connectome Project, WU-Minn Consortium (Principal Investigators: David Van Essen and Kamil Ugurbil; 1U54MH091657) funded by the 16 NIH Institutes and Centers that support the NIH

Blueprint for Neuroscience Research, and by the McDonnell Center for Systems Neuroscience at Washington University. *Conflicts of interest*: The authors report no conflicts of interest.

References

Anwander A, Tittgemeyer M, von Cramon DY, Friederici AD, Knösche TR. 2007. Connectivity-based parcellation of Broca's area. *Cereb Cortex*. 17(4):816–825.

Aron AR, Robbins TW, Poldrack RA. 2014. Inhibition and the right inferior frontal cortex: one decade on. *Trends Cogn Sci*. 18(4): 177–185.

Barbato G, Barini E, Genta G, Levi R. 2011. Features and performance of some outlier detection methods. *J Appl Stat*. 38(10):2133–2149.

Berretz G, Wolf OT, Güntürkün O, Ocklenburg S. 2020. Atypical lateralization in neurodevelopmental and psychiatric disorders: what is the role of stress? *Cortex*. 125:215–232.

Bradshaw JL, Sheppard DM. 2000. The neurodevelopmental frontostriatal disorders: evolutionary adaptiveness and anomalous lateralization. *Brain Lang*. 73(2):297–320.

Burt JB, Helmer M, Shinn M, Anticevic A, Murray JD. 2020. Generative modeling of brain maps with spatial autocorrelation. *NeuroImage*. 220:117038.

Cantalupo C, Hopkins WD. 2001. Asymmetric Broca's area in great apes. *Nature*. 414(6863):505–505.

Cao Z, Ottino-Gonzalez J, Cupertino RB, Schwab N, Hoke C, Catherine O, Cousijn J, Dagher A, Foxe JJ, Goudriaan AE, et al. 2016. Distinct global brain dynamics and spatiotemporal Organization of the Salience Network. *PLoS Biol*. 14(6):e1002469.

Chen T, Cai W, Ryali S, Supekar K, Menon V 2016. Distinct global brain dynamics and spatiotemporal organization of the salience network. *PLoS Biol*. 14:e1002469.

Corballis MC. 2017. The evolution of lateralized brain circuits. *Front Psychol*. 8:1021.

Cox RW. 1996. AFNI: software for analysis and visualization of functional magnetic resonance neuroimages. *Comput Biomed Res*. 29(3):162–173.

Crinion J, Turner R, Grogan A, Hanakawa T, Noppeney U, Devlin JT, Aso T, Urayama S, Fukuyama H, Stockton K. 2006. Language control in the bilingual brain. *Science*. 312(5779):1537–1540.

Di Martino A, Scheres A, Margulies DS, Kelly AM, Uddin LQ, Shehzad Z, Biswal B, Walters JR, Castellanos FX, Milham MP. 2008. Functional connectivity of human striatum: a resting state FMRI study. *Cereb Cortex*. 18(12):2735–2747.

Dice LR. 1945. Measures of the amount of ecologic association between species. *Ecology*. 26(3):297–302.

Estle SJ, Green L, Myerson J, Holt DD. 2006. Differential effects of amount on temporal and probability discounting of gains and losses. *Mem Cogn*. 34(4):914–928.

Fadiga L, Craighero L, D'Ausilio A. 2009. Broca's area in language, action, and music. *Ann N Y Acad Sci*. 1169(1):448–458.

Fallon JH, Ziegler BT. 1979. The crossed cortico-caudate projection in the rhesus monkey. *Neurosci Lett*. 15(1):29–32.

Garavan H, Ross TJ, Stein EA. 1999. Right hemispheric dominance of inhibitory control: an event-related functional MRI study. *Proc Natl Acad Sci USA*. 96(14):8301–8306.

Gershon RC, Cook KF, Mungas D, Manly JJ, Slotkin J, Beaumont JL, Weintraub S. 2014. Language measures of the NIH toolbox cognition battery. *J Int Neuropsychol Soc*. 20(6):642–651.

Glasser MF, Smith SM, Marcus DS, Andersson JL, Auerbach EJ, Behrens TE, Coalson TS, Harms MP, Jenkinson M, Moeller S. 2016. The human connectome project's neuroimaging approach. *Nat Neurosci*. 19(9):1175–1187.

Glasser MF, Sotiropoulos SN, Wilson JA, Coalson TS, Fischl B, Andersson JL, Xu J, Jbabdi S, Webster M, Polimeni JR. 2013. The minimal preprocessing pipelines for the human connectome project. *NeuroImage*. 80:105–124.

Goldman PS. 1978. Neuronal plasticity in primate telencephalon: anomalous projections induced by prenatal removal of frontal cortex. *Science*. 202(4369):768–770.

Goldman-Rakic PS. 1981. Prenatal formation of cortical input and development of cytoarchitectonic compartments in the neostriatum of the rhesus monkey. *J Neurosci*. 1(7):721–735.

Hampshire A, Chamberlain SR, Monti MM, Duncan J, Owen AM. 2010. The role of the right inferior frontal gyrus: inhibition and attentional control. *NeuroImage*. 50(3):1313–1319.

Jahanshahi M, Obeso I, Rothwell JC, Obeso JA. 2015. A fronto–striato–subthalamic–pallidal network for goal-directed and habitual inhibition. *Nat Rev Neurosci*. 16(12):719–732.

Joliot M, Jobard G, Naveau M, Delcroix N, Petit L, Zago L, Crivello F, Mellet E, Mazoyer B, Tzourio-Mazoyer N. 2015. AICHA: an atlas of intrinsic connectivity of homotopic areas. *J Neurosci Methods*. 254: 46–59.

Kelly C, Uddin LQ, Shehzad Z, Margulies DS, Castellanos FX, Milham MP, Petrides M. 2010. Broca's region: linking human brain functional connectivity data and non-human primate tracing anatomy studies. *Eur J Neurosci*. 32(3):383–398.

Knecht S, Drager B, Deppe M, Bobe L, Lohmann H, Floel A, Ringelstein EB, Henningsen H. 2000. Handedness and hemispheric language dominance in healthy humans. *Brain*. 123(Pt 12):2512–2518.

Korponay C, Choi EY, Haber SN. 2020. Corticostriatal projections of macaque area 44. *Cereb Cortex Commun*. 1(1):tgaa079.

Kucyi A, Hodaie M, Davis KD. 2012. Lateralization in intrinsic functional connectivity of the temporoparietal junction with salience- and attention-related brain networks. *J Neurophysiol*. 108(12): 3382–3392.

Lindell AK, Hudry K. 2013. Atypicalities in cortical structure, handedness, and functional lateralization for language in autism spectrum disorders. *Neuropsychol Rev*. 23(3):257–270.

Majid DA, Cai W, Corey-Bloom J, Aron AR. 2013. Proactive selective response suppression is implemented via the basal ganglia. *J Neurosci*. 33(33):13259–13269.

Mars RB, Verhagen L, Gladwin TE, Neubert FX, Sallet J, Rushworth MF. 2016. Comparing brains by matching connectivity profiles. *Neurosci Biobehav Rev*. 60:90–97.

Miyata J, Sasamoto A, Koelkebeck K, Hirao K, Ueda K, Kawada R, Fujimoto S, Tanaka Y, Kubota M, Fukuyama H, et al. 2012. Abnormal asymmetry of white matter integrity in schizophrenia revealed by voxelwise diffusion tensor imaging. *Hum Brain Mapp*. 33(7): 1741–1749.

Mwangi B, Tian TS, Soares JC. 2014. A review of feature reduction techniques in neuroimaging. *Neuroinformatics*. 12(2):229–244.

Myerson J, Green L, Warusawitharana M. 2001. Area under the curve as a measure of discounting. *J Exp Anal Behav*. 76(2):235–243.

Passingham RE, Stephan KE, Kotter R. 2002. The anatomical basis of functional localization in the cortex. *Nat Rev Neurosci*. 3(8): 606–616.

Postuma RB, Dagher A. 2006. Basal ganglia functional connectivity based on a meta-analysis of 126 positron emission tomography and functional magnetic resonance imaging publications. *Cereb Cortex*. 16(10):1508–1521.

Power JD, Barnes KA, Snyder AZ, Schlaggar BL, Petersen SE. 2012. Spurious but systematic correlations in functional connectivity MRI networks arise from subject motion. *NeuroImage*. 59(3):2142–2154.

Robles SG, Gatignol P, Capelle L, Mitchell M, Duffau H. 2005. The role of dominant striatum in language: a study using intraoperative electrical stimulations. *J Neurol Neurosurg Psychiatry*. 76(7):940–946.

Schel MA, Ridderinkhof KR, Crone EA. 2014. Choosing not to act: neural bases of the development of intentional inhibition. *Dev Cogn Neurosci*. 10:93–103.

Shepherd GM. 2013. Corticostriatal connectivity and its role in disease. *Nat Rev Neurosci*. 14(4):278–291.

Silk TJ, Vilgis V, Adamson C, Chen J, Smit L, Vance A, Bellgrove MA. 2016. Abnormal asymmetry in frontostriatal white matter in children with attention deficit hyperactivity disorder. *Brain Imaging Behav*. 10(4):1080–1089.

Simmonds DJ, Pekar JJ, Mostofsky SH. 2008. Meta-analysis of go/no-go tasks demonstrating that fMRI activation associated with response inhibition is task-dependent. *Neuropsychologia*. 46(1): 224–232.

Sommer I, Ramsey N, Kahn R, Aleman A, Bouma A. 2001. Handedness, language lateralisation and anatomical asymmetry in schizophrenia: meta-analysis. *Br J Psychiatry*. 178:344–351.

Swanson N, Eichele T, Pearlson G, Kiehl K, Yu Q, Calhoun VD. 2011. Lateral differences in the default mode network in healthy controls and patients with schizophrenia. *Hum Brain Mapp*. 32(4): 654–664.

Szaflarski JP, Binder JR, Possing ET, McKiernan KA, Ward BD, Hammeke TA. 2002. Language lateralization in left-handed and ambidextrous people: fMRI data. *Neurology*. 59(2):238–244.

Tan LH, Chen L, Yip V, Chan AH, Yang J, Gao J-H, Siok WT. 2011. Activity levels in the left hemisphere caudate–fusiform circuit predict how well a second language will be learned. *Proc Natl Acad Sci*. 108(6):2540–2544.

Uğurbil K, Xu J, Auerbach EJ, Moeller S, Vu AT, Duarte-Carvajalino JM, Lenglet C, Wu X, Schmitter S, Van de Moortele PF. 2013. Pushing spatial and temporal resolution for functional and diffusion MRI in the human connectome project. *NeuroImage*. 80: 80–104.

Van Essen DC, Smith SM, Barch DM, Behrens TE, Yacoub E, Ugurbil K, Consortium W-MH. 2013. The WU-Minn human connectome project: an overview. *NeuroImage*. 80:62–79.

Weintraub S, Dikmen SS, Heaton RK, Tulsky DS, Zelazo PD, Bauer PJ, Carlozzi NE, Slotkin J, Blitz D, Wallner-Allen K, et al. 2013. Cognition assessment using the NIH toolbox. *Neurology*. 80(11 Suppl 3):S54–S64.

Yan CG, Cheung B, Kelly C, Colcombe S, Craddock RC, Di Martino A, Li Q, Zuo XN, Castellanos FX, Milham MP. 2013. A comprehensive assessment of regional variation in the impact of head micromovements on functional connectomics. *NeuroImage*. 76: 183–201.

Zandbelt BB, Vink M. 2010. On the role of the striatum in response inhibition. *PLoS One*. 5(11):e13848.

Zelazo PD, Anderson JE, Richler J, Wallner-Allen K, Beaumont JL, Conway KP, Gershon R, Weintraub S. 2014. NIH toolbox cognition battery (CB): validation of executive function measures in adults. *J Int Neuropsychol Soc*. 20(6):620–629.